Impedance Recovery Python Script

Jakob Wenninger

January 20, 2020

Abstract

SIS junctions are used in astronomy to convert frequencies from hundred GHz magnitude (RF signal) to the low ten GHz regime (IF signal). The junction is embedded in a circuit which transmits the signal from the feedhorn to the junction. It is crucial for best performance, that the impedance is matched during this transmission. The presented software is able to compute the impedance of the SIS junction and of the circuit in which the junction is embedded. The script uses the direct current voltage (IV) response of the SIS junction to recover both impedances. A single IV response and the interaction of IV responses without and with AC power applied are computed in two separate classes. The obtained results for the embedding impedance are compared and agree within some margin with an existing software package, called QMix. In addition to the comparison with the existing software, the presented script has been tested on various DC bias voltage ranges from which the embedding impedance is recovered. The results indicate that the second photon step can be included in the impedance recovery and that the computation should also include data from negative DC bias voltages.

1 Introduction

Astronomical signals in the hundred GHz frequency regime are commonly detected using SIS mixer technology. The SIS junction down-converts the signal to a few GHz which can be processed using established technologies. The receiver chain is depicted in figure 1. The signal is collimated via the telescope or laboratory optics onto a feedhorn, which is mounted on the mixer block containing the mixer chip. On the mixer chip, there is an RF circuit, the SIS junction and an IF circuit. The RF circuit is fed with the high frequency signal from the feedhorn and the IF circuit transmits the down-converted signal to the readout electronics. The impedance of the signal needs to match at every single circuit element to avoid reflections of the signal. Within a circuit element, the impedance can change, so that the input impedance is not necessarily the output impedance.

The RF circuit is designed to match the impedance of the feedhorn at the RF circuit's input and to match the impedance of the SIS junction at the RF

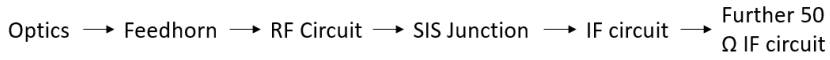

Figure 1: The path of the signal passes several stages where the RF circuit, the SIS junction and the IF circuit are located on the mixer chip.

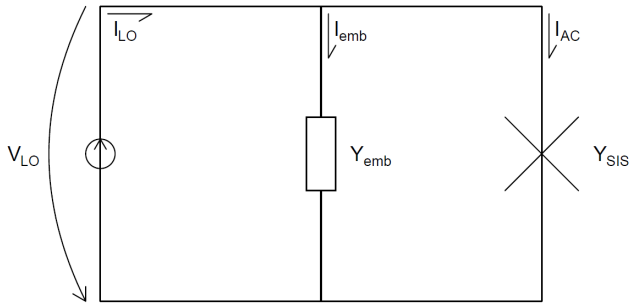

Figure 2: The Norton equivalent circuit of a Mixer chip has the embedding admittance parallel to the non-linear admittance of the SIS junction.

circuit's output. The impedance of the SIS junction is non-linear and depends on its dimensions, its materials and its direct current (DC) bias. In the same way, the IF input is required to meet the SIS junctions output impedance. The IF circuit output is usually required to match $50\,\Omega$, which is the standard impedance for industrial products as amplifiers.

In general, any circuit can be replaced by a Norton equivalent circuit or Thevenin equivalent circuit. A Thevenin equivalent circuit consist of a voltage source and a series resistance, and the Norton equivalent circuit consist of a current source and a parallel resistance. This report uses the Norton equivalent circuit which is shown in figure 2. The telescope optics, feedhorn and RF circuit are represented by a current source and a parallel admittance, called embedded admittance. The SIS junction is represented by a parallel admittance. In the simplest case, the circuit is fed by a single frequency, the local oscillator signal (LO).

From measurements of the DC current voltage (IV) response of the SIS junction, it is possible to recover the embedding admittance. The IV response forms so called photon steps as LO power is applied. The IV response without LO power is referred to as unpumped IV response, and the IV response with LO power applied is called pumped IV response. An example for an unpumped and pumped IV response is shown in figure 3. These two DC responses are sufficient to compute the AC current and voltage of the SIS junction branch of the Norton equivalent circuit. Consequently, the admittance of the SIS junction can be computed following the flowchart in figure 4. The admittance of the SIS junction is evaluated at every DC bias voltage to linearise the admittance, since the admittance of the SIS junction is intrinsically non-linear. Finally, the remaining characteristics of the Norton equivalent circuit can be computed

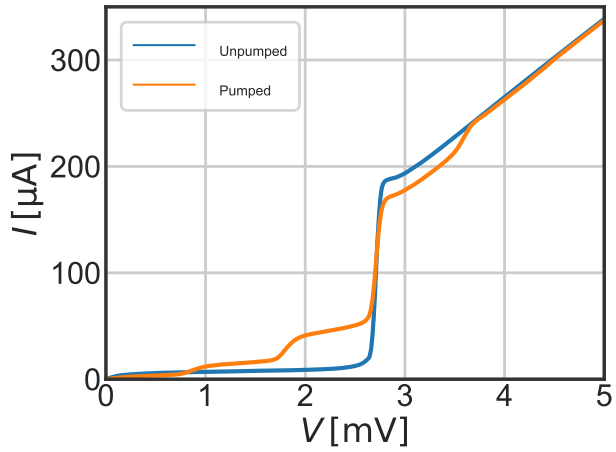

Figure 3: The unpumped IV curve has no RF power applied, while the pumped IV curve is driven with an RF signal.

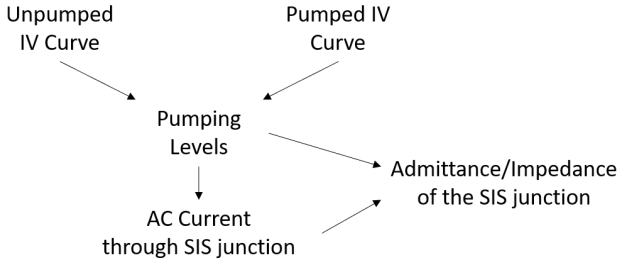

Figure 4: The AC quantities of the SIS junction branch of the Norton equivalent circuit is determined following this flow chart.

knowing the AC characteristics of the SIS junction branch.

The following section describes the theory on which the admittance recovery is based. The method section describes the computation involved in the admittance recovery and how the theory is put into practise. Finally, the results are presented and discussed.

2 Theory

The theory of quasiparticle tunnelling in SIS junctions is described by Tucker and Feldman [1985]. The unpumped and pumped DC IV response are connected

by

$$I(V_0, V_{\mathrm{LO}}) = \sum_{n=-\infty}^{\infty} J_n^2(\alpha) \cdot I_0(V_0 + n \cdot V_{\mathrm{Ph}}) \tag{1}$$

where I_0 is the unpumped DC IV curve, I is the pumped DC IV curve and J_n is the n^{th} order Bessel function of first kind evaluated at the normalised pumping level $\alpha = V_{\mathrm{LO}}/V_{\mathrm{Ph}}$. The photon voltage V_{Ph} is given by the frequency f_{LO} of the pump following

$$V_{\mathrm{Ph}} = \frac{h \cdot f_{\mathrm{LO}}}{e}, \tag{2}$$

where h is Planck's constant and e is the electron charge.

The AC current through the SIS junction can be calculated knowing the pumping level. The real part is

$$Re\{I_{\mathrm{AC}}(V_0, V_{\mathrm{LO}})\} = \sum_{n=-\infty}^{\infty} J_n(\alpha) \cdot (J_{n-1}(\alpha) + J_{n+1}(\alpha)) \cdot I_0(V_0 + n \cdot V_{\mathrm{Ph}}), \tag{3}$$

and the imaginary part is

$$Im\{I_{\mathrm{AC}}(V_0, V_{\mathrm{LO}})\} = \sum_{n=-\infty}^{\infty} J_n(\alpha) \cdot (J_{n-1}(\alpha) - J_{n+1}(\alpha)) \cdot I_{\mathrm{KK}}(V_0 + n \cdot V_{\mathrm{Ph}}). \tag{4}$$

I_{KK} is the Kramers Kronig transformation of the unpumped IV curve I_0, a special case of the Hilbert transformation.

Since the pumping level voltage and the AC current through the SIS junction are known, the admittance and impedance of the SIS junction can be computed as a linearisation of the junction at every bias voltage

$$Y_{\mathrm{SIS}}(V_0) = \frac{I_{\mathrm{AC}}(V_0)}{V_{\mathrm{LO}}(V_0)} \ . \tag{5}$$

The calculations above describe the branch of the SIS junction in the Norton equivalent circuit. The unknown quantities of the circuit, the current from the LO source I_{LO}, the current through the embedding admittance, and the embedding admittance Y_{Emb}, can be determined since the circuit equation

$$I_{\mathrm{LO}} - I_{\mathrm{AC}}(V_0) = V_{\mathrm{LO}}(V_0) \cdot Y_{\mathrm{Emb}} \tag{6}$$

needs to hold for all bias voltages V_0. In fact, I_{LO} is determined by

$$I_{\mathrm{LO}} = V_{\mathrm{LO}} \cdot (Y_{\mathrm{Emb}} + Y_{\mathrm{SIS}}) \ . \tag{7}$$

In consequence, the only unknown quantity of the Norton equivalent circuit is the embedding admittance.

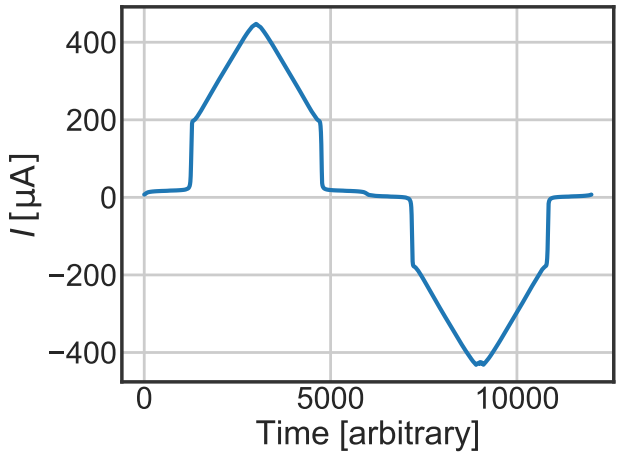

Figure 5: The IV data is recorded by sweeping the voltage up and down, starting close to 0 V. The time axis shows the indexes of the IV entries in the `.csv` file.

3 Methods

Data from the unpumped and pumped IV curves is necessary to perform the admittance recovery. The computation of a single IV response and the computation of the interaction of the IV responses can be separated. The computation of a single IV dataset is described in the following IV Response section 3.1. In the Mixer section 3.2, the computation of the admittance recovery is described. Both, the IV Response section and the Mixer section, correspond to separate classes coded in Python.

3.1 IV Response

3.1.1 Data Handling

The `IV_Response` class handles a single IV dataset. Experimentally, these datasets are obtained by sweeping the voltage up and down to conserve hysteresis behaviour. The voltage sweeping limits, the number of data points and a few other parameters depending on the experimental setup are controlled with a Labview readout program. The program stores data in `.csv` files. The `IV_Response` class reads the dataset from a location defined by the user.[1] The current data sorted by their index in figure 5 shows the sweep behaviour.

The first data processing step is the correction of the current and voltage

[1] There are keyword arguments (`headerLines`, `footerLines`, `columnOffset`) to specify the layout of the `.csv` file. The only requirement is that the file contains a column with voltage data stored next to current data. The unit of the current data can be specified with the keyword argument `currentFactorToMicroampere`.

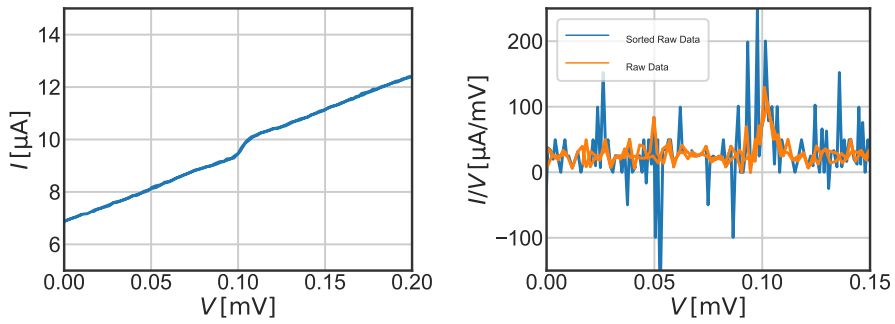

(a) At the true origin, the IV curve shows a transition between negative and positive subgap current. The transition has a slightly larger slope.

(b) The offset can be found as peaks in the slope between the data points of the raw dataset, which contains the sweep in positive and negative voltage direction. Sorting the dataset by increasing voltage introduces artificial peaks in the slope. For this reason, the offset is determined from the unmodified 'raw' IV dataset.

Figure 6: The recorded IV dataset shows an offset in voltage and current.

offset.[2] At the origin, the IV curve shows a larger slope than in the remaining subgap region as shown in figure 6. For this reason, the slope of the raw data is computed. The largest two slopes originate from the sweep with positive and negative voltage gradient.[3] The voltages of the peaks are averaged and interpreted as voltage offset. The current offset is determined from the average of the currents at the two voltage values in the IV dataset closest to the voltage offset.

Subsequently, the dataset is sorted by increasing voltage. The slope of the sorted dataset is distorted as shown in figure 6 and is therefore not suitable for offset determination. The effect on the path of the IV curve at the transition is shown in figure 7. The sorted dataset is smoothed with a Savitzky-Golay filter to average the hysteresis behaviour.[4]

The filtered data is then allocated in equispaced voltage bins to avoid complications at later stages, especially in dealing with both the unpumped and pumped IV curves.[5] The effect of binning the filtered data instead of the voltage sorted dataset is shown in figure 8.

[2]The offset correction can be skipped by entering the offset in the keyword argument `fixedOffset`.

[3]The voltage offset is searched within a voltage range determined by the keyword argument `offsetThreshold`.

[4]The Savitzky-Golay filter is part of the `scipy.signal` package. Its parameters are accessible via the keyword arguments `savgolWindow` and `savgolOrder`.

[5]The parameters for binning the data are interfered by the keyword arguments `numberOfBins`, `vmin` and `vmax`.

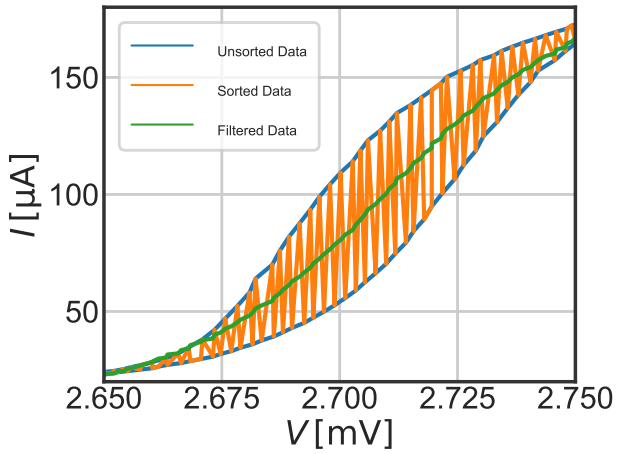

Figure 7: The data is recorded by sweeping the voltage up and down to include hysteresis behaviour. Sorting the dataset after increasing voltage leads to rapid fluctuations of the IV curve, especially at the transition. This sorted dataset is filtered with Savitzky-Golay filter to obtain a smooth IV curve representing an average of the hysteresis.

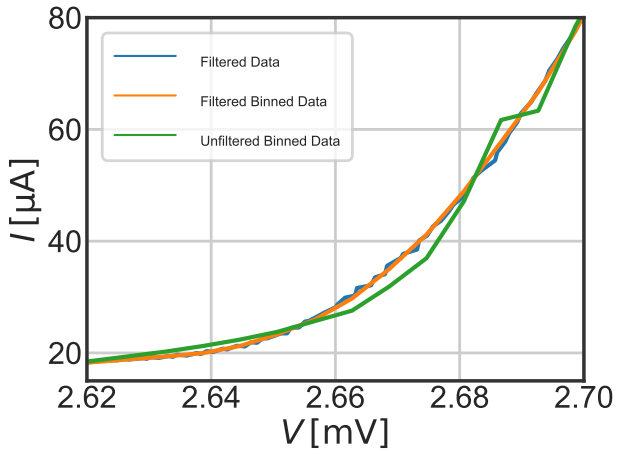

Figure 8: The Savitzky-Golay filtered IV curve shows some minor fluctuations. The filtered dataset is binned into equispaced voltage bins to smoothen these fluctuations and to obtain an equispaced voltage axis. Binning of the unfiltered data leads to artificial steps in the IV response.

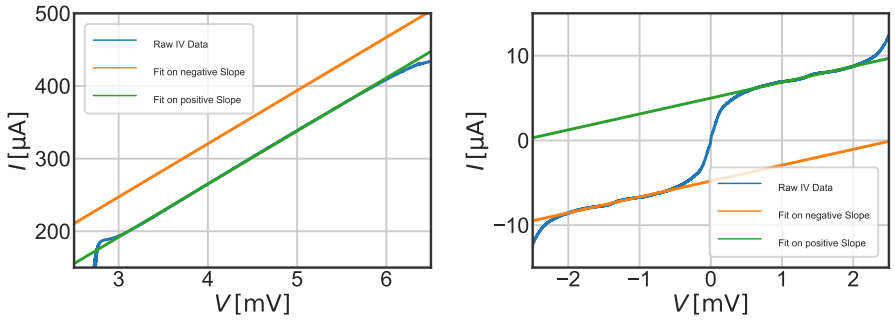

(a) The linear regression through the normal resistance regime.

(b) The linear regression through the subgap resistance regime.

Figure 9: The linear regressions are performed separately for negative and positive bias voltages.

3.1.2 Determination of Characteristic Values

The characteristic values of the IV response are determined after processing the dataset. The normal and subgap resistance are determined through linear regression of the offset corrected raw data sorted by increasing voltage within the corresponding voltage ranges.[6] Separate fits through the negative and positive bias regime are performed, then averaged. The errors of the linear regressions are propagated to an error of the normal and subgap resistance respectively. The linear regressions are shown in figure 9.

The gap voltage is determined from the maximum slope of the binned IV data at the transition voltage regime.[7] Figure 8 shows negligible fluctuations in the binned IV dataset in comparison to the Savitzky-Golay filtered dataset. The effect on the slope is shown in figure 10. The maximum slopes at negative and positive bias voltages are averaged to obtain the gap voltage.[8]

The critical current is determined from the normal resistance and the gap voltage as

$$I_{\mathrm{C}} = \frac{V_{\mathrm{gap}}}{R_{\mathrm{N}}}, \tag{8}$$

where V_{gap} is the gap voltage and R_{N} is the normal resistance. Alternatively, the critical current can be determined from the current after the transition. Liu et al. [2017] described the critical current as

$$I_{\mathrm{C}} = I_{\mathrm{gap}} \cdot \frac{\pi}{4}, \tag{9}$$

[6] The voltage ranges used for the linear regression are adjustable by the keyword arguments `rNThresholds` and `rSGThresholds`

[7] The voltage regime evaluated for the determination of the gap voltage is accessible via the keyword argument `vGapSearchRange`.

[8] A suggested improvement would involve the fit of a gaussian on the transition and using its peak as gap voltage. However, this would be accompanied by a computationally more intense fitting.

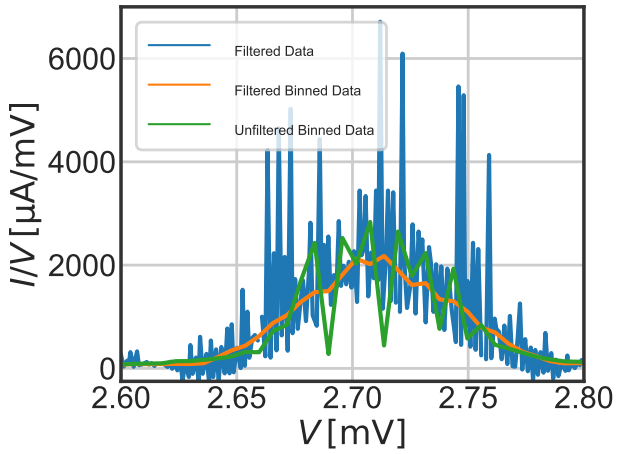

Figure 10: The maximum slope at the transition is used to determine the gap voltage. The Savgol-Golay filtered dataset and the unfiltered dataset show strong fluctuations. Binning of the Savgol-Golay filtered dataset leads to a smooth IV response and minimum fluctuations in its slope.

where I_{gap} is the current after the transition. This current is determined by the first negative slope in the binned IV data after the gap voltage.

3.1.3 Simulated IV Response

The characteristic values determine an IV response. For calculations involving certain portions of the IV curve, a simulated IV response with a larger number of data points can be convenient. In that case, the IV response is described by a model with certain parameters instead of the IV curve's characteristic values. The `IV_Response` class has several models implemented. The currently implemented methods are based on two approaches, namely the Chalmers approach and the gaussian convolution approach.

The Chalmers approach uses the equation

$$\begin{aligned} I(V) = \; & \frac{V}{R_{\mathrm{SG}}} \cdot \left(1 + \mathrm{e}^{-a\cdot(V+V_{\mathrm{gap}})}\right)^{-1} + \frac{V}{R_{\mathrm{N}}} \cdot \left(1 + \mathrm{e}^{a\cdot(V+V_{\mathrm{gap}})}\right)^{-1} \\ & + \frac{V}{R_{\mathrm{SG}}} \cdot \left(1 + \mathrm{e}^{a\cdot(V-V_{\mathrm{gap}})}\right)^{-1} + \frac{V}{R_{\mathrm{N}}} \cdot \left(1 + \mathrm{e}^{-a\cdot(V-V_{\mathrm{gap}})}\right)^{-1} \end{aligned} \tag{10}$$

presented by Rashid et al. [2016] with the fitting parameter a. The fit shown in figure 11 shows good agreement in describing the transition, but bad fitting of the subgap regime.

The gaussian convolution method is implemented for a better description of the subgap resistance. The idea of this method is to convolve a perfect IV curve with a gaussian of a certain width. The parameters of this model involve the

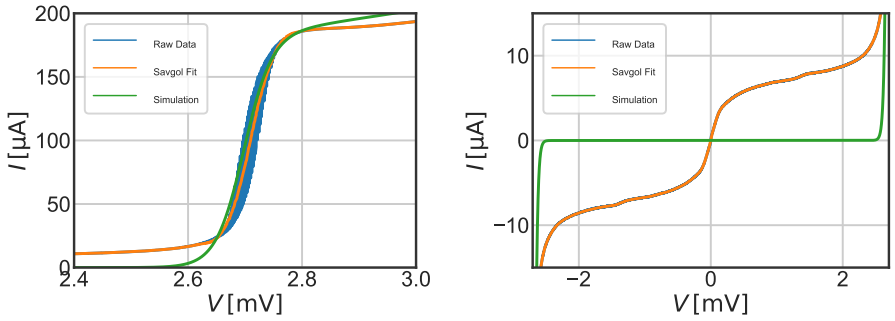

Figure 11: The Chalmer approach leads to good agreement with the data in the transition region. In the subgap region, however, the simulation agrees badly with the data.

width of the gaussian and the parameters of the IV curve. The simplest IV curve has no subgap leakage, a step function at the transition and a normal resistance slope afterwards as shown in figure 12. A subgap current can be included by a constant non-zero value in the subgap region as shown in figure 13. The constant corresponds to a step function at 0 V. An even better agreement of the model with the data is achieved by including a subgap resistance slope as shown in figure 14. Finally, efforts in optimising the description of regions just before and after the transition led to include an excess current at the transition to the model, shown in figure 15.

There are different methods implemented to fit the presented models convolved with a gaussian to the Savitzky-Golay filtered data. Best performance is achieved with a stepwise fit, where the parameters are adjusted at the voltage regime they have most impact on. For example, the subgap leakage parameters are fitted in the same region as the subgap resistance is determined. The simulation and the Savitzky-Golay filtered data are shown in figure 16.

3.2 Mixer

The unpumped and pumped IV responses are used to determine the embedding admittance of the mixer. The `Mixer` class connects the `IV_Response` objects of the unpumped and pumped IV datasets to perform this calculation.[9]

3.2.1 AC Characteristic of the SIS Junction Branch

In the first step, equation 1 is used to evaluate the pumping level at all bias voltages V_0. Consequently, the pumping level is a function of the bias voltage $\alpha(V_0)$ as shown in figure 17. This calculation requires the unpumped IV curve to be evaluated at bias voltages $V_0 + n \cdot V_{\mathrm{Ph}}$, where n runs in theory from

[9] The unpumped and pumped `IV_Response` objects are the `Unpumped` and `Pumped` arguments in the `Mixer` object.

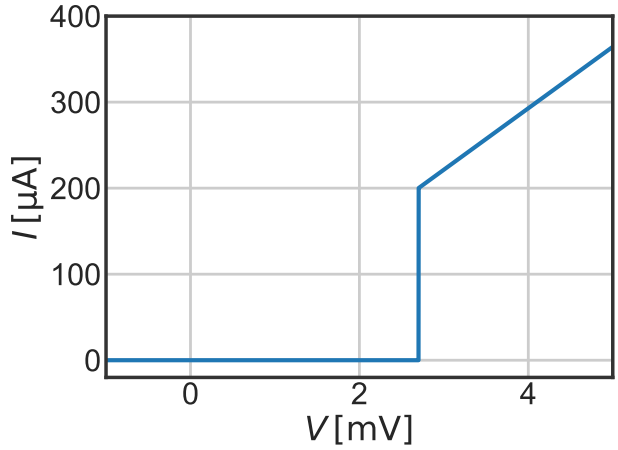

Figure 12: The model of a perfect IV reponse has no subgap current and a step function at the gap voltage followed by a normal resistance slope.

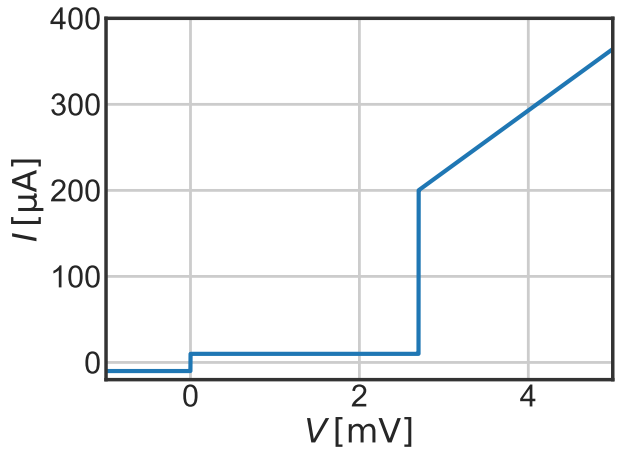

Figure 13: The model of a perfect IV curve can be expanded by including a finite constant subgap current.

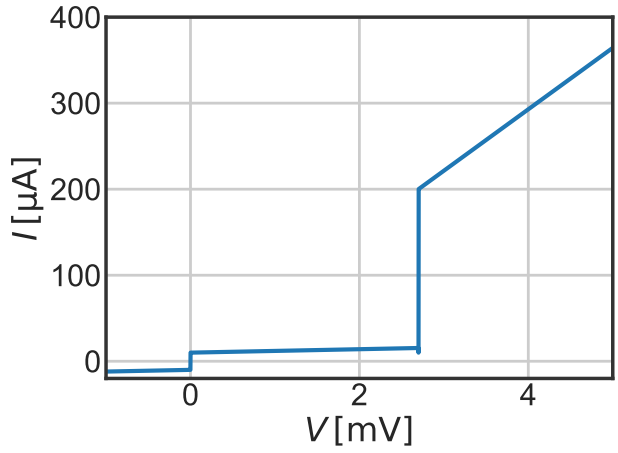

Figure 14: The subgap region of a perfect IV curve can be modelled with a subgap resistance and a step function at the origin.

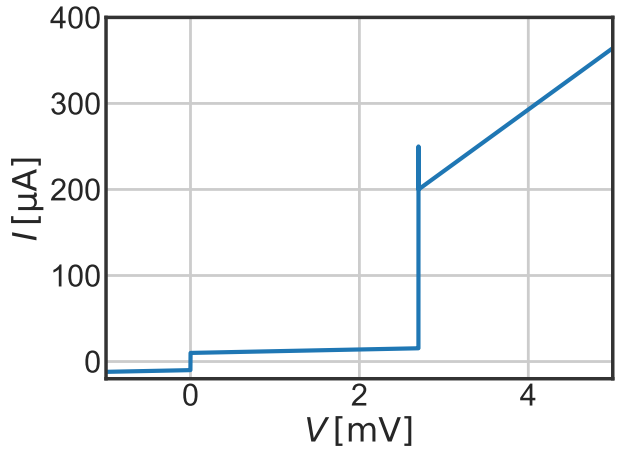

Figure 15: The perfect IV curve model with subgap current simulation can be expanded by a excess current at the transition, to improve the fit at bias voltages close to the transition after the convolution with a gaussian.

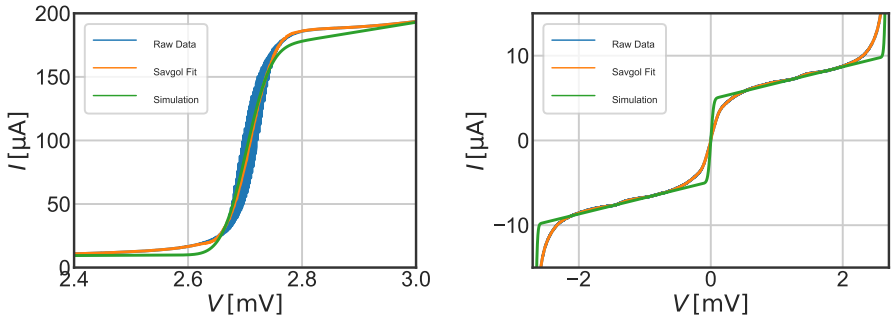

Figure 16: The convolution of a gaussian with an IV curve with subgap current offset, subgap resistance and an excess current at the transition leads to good agreement with the data.

$-\infty$ to $+\infty$. The photon voltage is determined from the pumping frequency f_{LO} following equation 2.[10] In fact, n is limited to a finite value for effective computation, since the multiplicative value of the Bessel function J_n vanishes at larger values of n.[11] The unpumped IV curve data needs to be expanded to larger voltages to be able to evaluate the unpumped data at $V_0 + n \cdot V_{\mathrm{Ph}}$. This is done with the information of the junctions normal resistance. Likewise, the Kramers Kronig transformation of the unpumped IV curve uses this expanded voltage regime.[12]

The expanded unpumped IV curve and the corresponding Kramers Kronig transformation in conjunction with the pumping level are used to compute the AC current through the SIS junction following equation 3 and 4.[13] The AC current through the SIS junction, evaluated at every bias voltage, is shown in figure 18.

The admittance of the SIS junction can be linearised for every bias voltage following equation 5. The admittance and the impedance, which is the reciprocal of the admittance, are shown in figure 19.

3.2.2 Embedding Admittance Recovery

The embedding admittance is computed from the first photon steps of the quantities computed above.[14] The width of the photon step is V_{Ph}, and the photon steps are counted from the gap voltage into the subgap region. Figure 20 shows

[10] The pumping frequency f_{LO} is given by the keyword argument `fLO`.

[11] The summation index is accessible via the keyword argument `tuckerSummationIndex`.

[12] The expansion and Kramers Kronig transformation is done within the `IV_Response` object of the unpumped IV data.

[13] The methods `iACSISRe_Calc` and `iACSISIm_Calc` are used to compute the arguments `iACSISRe` and `iACSISIm`. The results are concatenated to the complex AC current `iACSIS`.

[14] The number of photon steps involved is determined by the keyword argument `steps_ImpedanceRecovery`.

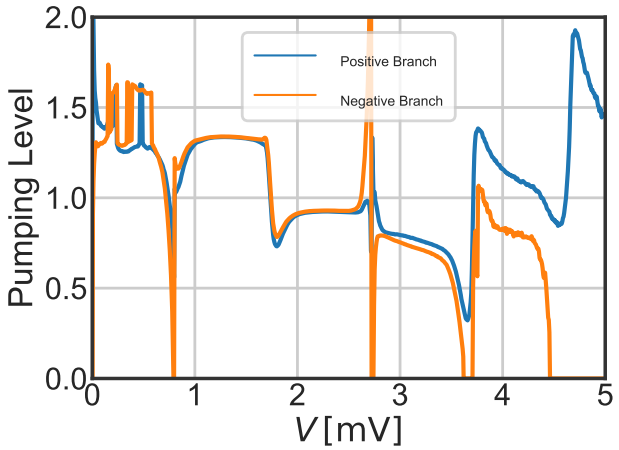

Figure 17: The pumping level is evaluated from the unpumped and pumped IV response at every single bias voltage. The pumping level from negative bias voltages is close to the pumping level of the corresponding positive bias voltages.

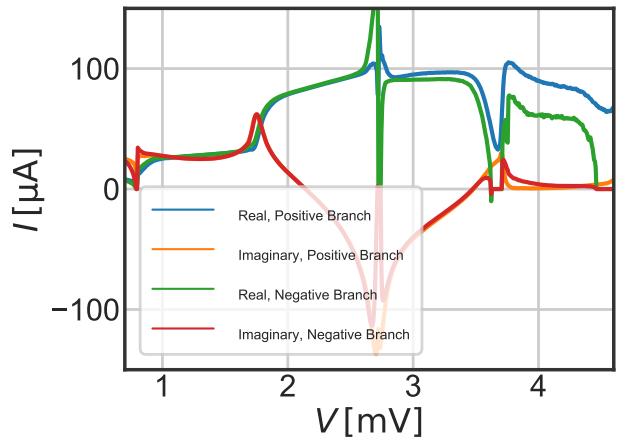

Figure 18: The real and imaginary AC current are calculated from the pumping level at every bias voltage. Both negative and positive bias voltages are displayed.

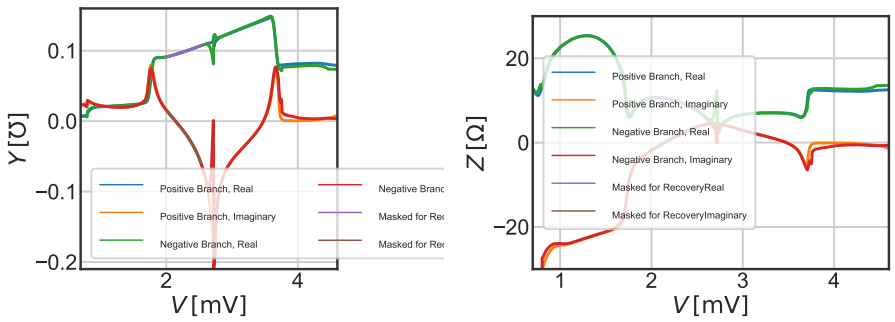

Figure 19: The embedding admittance and impedance show an almost linear response at the first photon step.

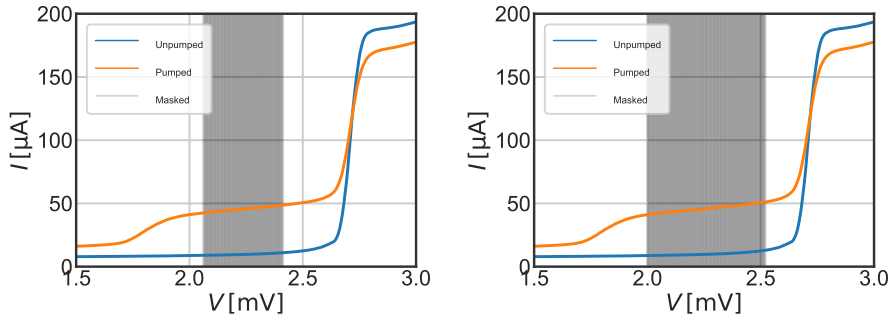

(a) This method uses a gaussian fit on the transition of the IV curve.

(b) This method uses boundaries defined by the user.

Figure 20: The bias voltages of the first photon step used for the admittance recovery can be selected using two methods.

the two masking strategies applied on the first photon step.[15] In general, parts close to the boundary of the photon step are excluded from processing, since there is a transition between the single photon steps and the transition of the IV curve itself. These effects arise from the fact that the tunnelling of quasi-particles through the SIS junction is a probability function. The first masking strategy excludes a certain voltage range at the boundary of the photon step, similar to the QMix package. The second masking strategy fits the slope of the transition of the IV curve with a gaussian as shown in figure 21. The masked voltage range is the photon step width reduced by four times the width of this gaussian fit on each side.

The embedding admittance is then recovered using the masked quantities of the SIS junctions branch in the Norton equivalent circuit. This is possible

[15]The used masking strategy and its parameters are accessible via the keyword argument `maskingWidth`.

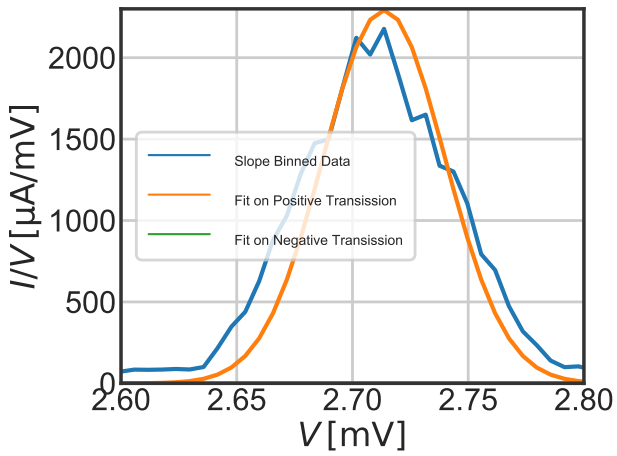

Figure 21: The slope of the transition is fitted with a gaussian. The width of the gaussian is used for one of the masking methods.

since the circuit equation 6 needs to hold for all bias voltages V_0. The problem becomes a minimisation problem since the data is noisy. The class contains different cost functions associated with the minimisation problem, but they lead to similar result. In general, there are two kinds of cost functions, those with the I_{LO} as a parameter and those which compute I_{LO} from the embedding admittance using equation 7.[16] Numerically, I_{LO} is obtained from

$$I_{\mathrm{LO}} = \frac{\sum_i \frac{V_{\mathrm{LO},i}}{\sqrt{(Y_{\mathrm{LO}}+Y_{\mathrm{SIS},i})^2_{Re}+(Y_{\mathrm{LO}}+Y_{\mathrm{SIS},i})^2_{Im})}}}{\sum_i (Y_{\mathrm{LO}}+Y_{\mathrm{SIS},i})^2_{Re}+(Y_{\mathrm{LO}}+Y_{\mathrm{SIS},i})^2_{Im})^{-1}} \tag{11}$$

following Skalare [1989].[17]

Skalare [1989] describes the 'Eyeball' method as a straightforward embedding admittance recovery method.[18] This method validates the circuit equation 6 for a guessed Y_{emb} and I_{LO} to obtain the pumping level. The pumping level is then used to compute a pumped IV curve which is compared with the measured pumped IV curve. This concept is computationally intense, since the AC current through the SIS junction depends on the pumping level and the pumping level computation is a separate minimisation during each evaluation of the Eyeball cost function.

[16] Both methods are implemented for all cost functions.

[17] The corresponding method is called `current_LO_from_Embedding_Circuit`.

[18] The corresponding method is called `yEmb_from_circuit`. Note that in this method I_{LO} is required to be a fitting parameter.

The second method described by Skalare minimises[19]

$$\begin{aligned}\text{Cost Skalare} = &\sum_i V_{\mathrm{LO},i}^2 \\ &+ |I_{\mathrm{LO}}|^2 \cdot \sum_i \left((Y_{\mathrm{LO}} + Y_{\mathrm{SIS},i})_{Re}^2 + (Y_{\mathrm{LO}} + Y_{\mathrm{SIS},i})_{Im}^2\right)^{-1} \\ &- 2 \cdot |I_{\mathrm{LO}}| \cdot \sum_i \frac{V_{\mathrm{LO},i}}{\sqrt{(Y_{\mathrm{LO}} + Y_{\mathrm{SIS},i})_{Re}^2 + (Y_{\mathrm{LO}} + Y_{\mathrm{SIS},i})_{Im}^2)}} \ .\end{aligned} \tag{12}$$

Another method determines the pumping level from I_{LO} and the total admittance of the circuit, and compares the result with the pumping level determined from the unpumped and pumped IV curve. The corresponding cost function is

$$\text{yEmb\_cost\_Function} = \sum_i \left(V_{\mathrm{LO},i} - \left|\frac{I_{\mathrm{LO}}}{Y_{\mathrm{LO}} + Y_{\mathrm{SIS},i}}\right|\right)^2 . \tag{13}$$

In equation 12 and 13, I_{LO} can be a minimisation quantity or it is determined from equation 11.[20] Note that I_{LO} is an absolute quantity.

The impedance recovery described by Withington et al. [1995] is implemented as

$$\text{zEmb\_cost\_Function} = \sum_i |V_{\mathrm{LO},i}|^2 \, 2 - \frac{\left(\sum_i \left|\frac{Z_{\mathrm{SIS},i}}{Z_{\mathrm{emb}}+Z_{\mathrm{SIS},i}} \cdot V_{\mathrm{LO},i}\right|\right)^2}{\left(\sum_i \left|\frac{Z_{\mathrm{SIS},i}}{Z_{\mathrm{emb}}+Z_{\mathrm{SIS},i}}\right|\right)^2} \tag{14}$$

where $Z_{\mathrm{SIS}}(V_0) = Y_{\mathrm{SIS}}^{-1}(V_0)$.[21] The same minimisation strategy has been used by the QMix package.

In the case where I_{LO} is not determined during the minimisation, it is computed from equation 11.

3.2.3 Evaluation of the Embedding Impedance Result

The result for the embedding admittance is finally evaluated following the steps shown in figure 22. The pumping level at every single bias voltage V_0 is computed by minimising the cost function

$$\text{cost\_vLO\_from\_circuit} = \left||I_{\mathrm{LO}}|^2 - |I_{\mathrm{AC}}(V_0, V_{\mathrm{LO}}) + Y_{\mathrm{Emb}} \cdot V_{\mathrm{LO}}|^2\right| . \tag{15}$$

This pumping level is then used in conjunction with equation 1 to compute a recovered pumped IV curve from the unpumped IV curve. This curve is compared with the measured pumped IV curve as shown in figure 23.

[19] The corresponding methods are `findYemb_Skalare` and `findYemb_Skalare_fixed_iLO` which computes the I_{LO} internally.

[20] The corresponding methods are `findYemb` and `findYemb_ILO` which computes the I_{LO} internally.

[21] The corresponding method is `findZemb`.

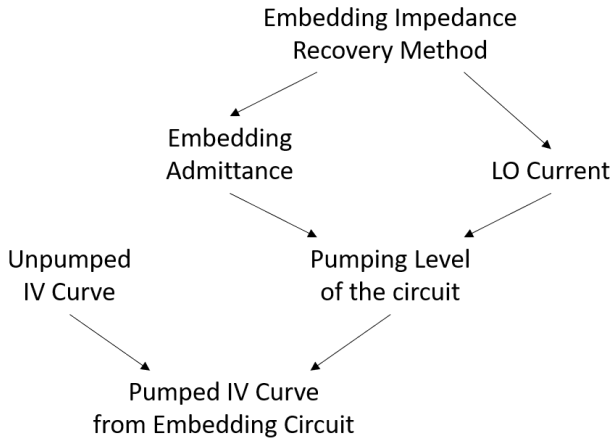

Figure 22: The result of the embedding admittance can be used to reconstruct the pumped IV curve following this flowchart.

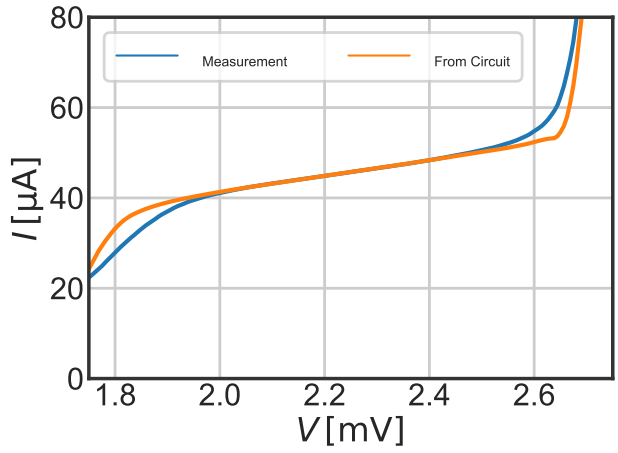

Figure 23: The pumped IV curve computed from the embedding impedance shows good agreement with the measured pumped IV curve over the voltage range of the first photon step. The embedding impedance recovery utilised the gaussian masking strategy.

	Obtained Result	QMix Result
Gap Voltage [mV]	2.71	2.72
Normal Resistance [Ω]	13.68	13.41
Subgap Resistance [Ω]	533.7	364.50
Voltage Offset [mV]	0.10	0.10
Current Offet [μA]	9.62	9.67

Table 1: The results of the unpumped IV curve are similar to the QMix results.

4 Results

The presented software has been tested with example data from the QMix package to validate the results with the QMix results. Since the QMix package uses one photon step for the impedance recovery, the presented results are obtained from the first photon step unless otherwise stated.

The characteristics of the unpumped IV response obtained with the QMix package and the presented software are compared in table 1. The results agree in all parts except for the subgap resistance. This can be ascribed to the voltages from which the subgap resistance is obtained. QMix determines the subgap resistance at 2.0 mV, while the presented software obtains the subgap resistance from a linear regression between 1.2 mV and 1.8 mV. The subgap resistance of the `IV_Response` object results in 368.2 Ω by setting the limits for the linear regression to 1.9 mV and 2.1 mV. This agrees with the QMix result.

The QMix package's impedance recovery follows Withington et al. [1995] and results without modifications in $(6.30 - 4.02j)\,\Omega$ which corresponds with an embedding admittance of $(0.1128 + 0.0720j)\,\mho$. The QMix package evaluates the impedance at a defined set of resistances and reactances so that the result changes to $(6.45 - 4.21j)\,\Omega$ after increasing the number of evaluated resistances and reactances by a factor of 50 each.[22] The pumped IV curve in figure 24 is recovered from the QMix's embedding impedance result plugged into the `Mixer` class using pumping levels from the fixed voltage masking strategy with the same voltage limits as in the QMix package. The plot also shows the result obtained with the presented software which is closer to the measured data.

The presented script uses two different masking strategies where the photon step extent is either reduced by four times the width of the gaussian fit on the transition or by a defined width. A comparison of the results for the masking strategies is shown in figure 25. Furthermore, there is a difference between including data from only positive bias voltages, and including the data at photon steps with negative bias voltage. This is shown in figure 26. The results for both masking strategies are presented in table 2. The results of the Skalare method,

[22] The result requires changes in the `RawData` class of the QMix package under the path `qmix/exp/exp_data.py`.

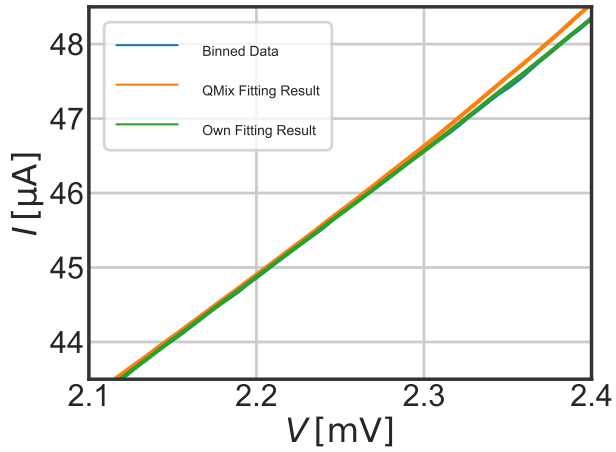

Figure 24: The pumped IV curves computed from the QMix result and the here presented fitting methods agree well with the measured pumped IV response at the first photon step. The photon step is masked with the fixed voltage masking strategy and the limits used by the QMix package. Note that the blue Binned Data curve is mostly covered by the green line.

the Withington method, and the circuit evaluation method are consistent with the cost functions described in equations 12, 14 and 13, respectively. For example, where the eyeball method results in $(0.0669 + 0.0617j)\,\mho$ or $(8.08 - 7.45j)\,\Omega$ respectively, the other methods result in $(7.67 - 5.66j)\,\Omega$. This originates from the different approach for the eyeball method. However, the comparison of the resulting pumped IV curves in figure 27 shows minor differences in the fitting region. There are two possibilities to explain the low difference between the results. Either the shape of the pumped IV curve is insensitive to the difference of the embedding admittance, or the evaluation of the pumped IV curve is chosen improperly.

Finally, there is the possibility to use the second photon step in addition to the first photon step as shown in figure 28. In general, the second photon step is considered too noisy to perform the embedding admittance recovery on this data. Figure 17, however, shows a well defined pumping level in the region of the second photon step. The results for the embedding admittance obtained with both masking strategies over two photon steps are presented in table 3. Figure 29 shows good agreement between the measurement and the recovered pumped IV curve. Interestingly, the result, which includes the data at bias voltages between the first and second photon step, shows good agreement at the photon steps themselves and shows better agreement at the voltages between the photon steps. In conclusion, the results obtained by including two photon steps show better agreement with the pumped IV curve than the results obtained from one photon step.

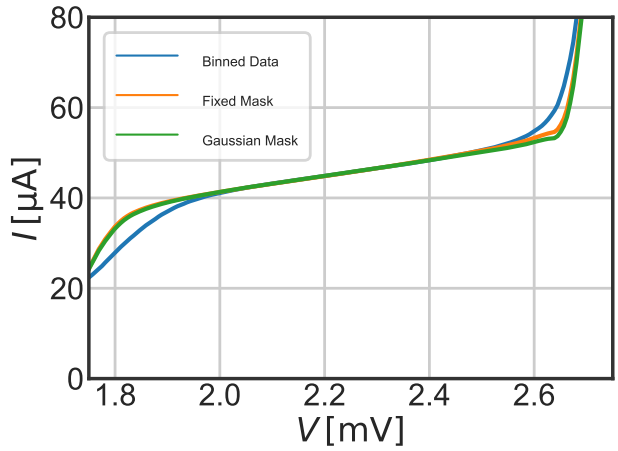

Figure 25: The pumped IV curve computed from the fixed voltage masking strategy shows slightly better agreement close to the transition than the gaussian masking strategy. This can be ascribed to the fact that the fixed voltage masking strategy includes voltages beyond 2.5 mV while the gaussian masking strategy includes voltages only up to 2.41 mV.

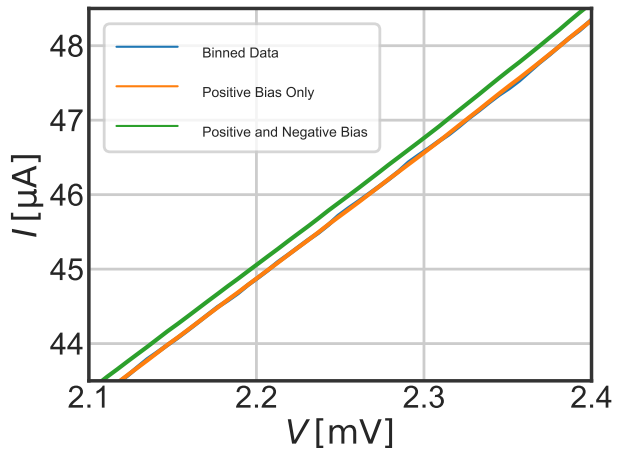

Figure 26: The pumped IV curve computed from the masked photon step at positive bias voltages shows good agreement with the binned IV curve in the positive voltage range. The recovered binned IV curve from results obtained in negative and positive bias voltage regions is offset, since the pumping level at negative bias voltages is of slightly larger magnitude.

Pos. and Neg. Voltages	Gaussian Masking Limits		Defined Masking Limits	
	Y_{emb} [℧]	I_{LO} [µA]	Y_{emb} [℧]	I_{LO} [µA]
Skalare	0.0844 + 0.0623j	166.8	0.1033 + 0.0703j	184.7
Cost Function	0.0844 + 0.0623j	166.2	0.1033 + 0.0703j	184.7
Eyeball	0.0669 + 0.0617j	152.0	0.1311 + 0.0771j	209.4
Withington	0.0844 + 0.0623j		0.1033 + 0.0703j	
Positive Voltages	Gaussian Masking Limits		Defined Masking Limits	
	Y_{emb} [℧]	I_{LO} [µA]	Y_{emb} [℧]	I_{LO} [µA]
Skalare	0.0793 + 0.0604j	161.5	0.0950 + 0.0675j	176.5
Cost Function	0.0793 + 0.0604j	161.5	0.0950 + 0.0675j	176.5
Eyeball	0.0687 + 0.0572j	151.8	0.0940 + 0.0665j	175.4
Withington	0.0793 + 0.0604j		0.0950 + 0.0675j	

Table 2: The results of the different evaluation methods are listed for both masking strategies, where in the upper panel positive and negative bias voltages are used, and only positive bias voltages are evaluated in the lower panel results.

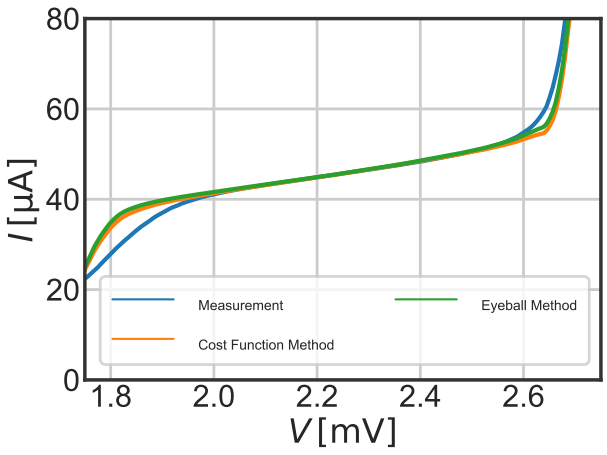

Figure 27: The pumped IV curves computed with the cost function methods and the eyeball method show similar results and good agreement with the measured IV curve.

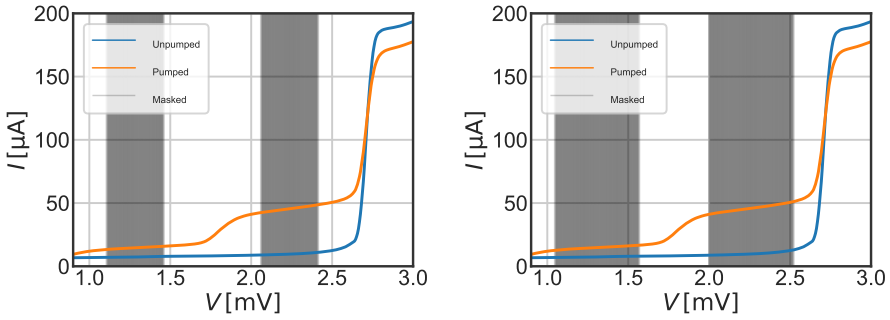

(a) The evaluated bias voltage region originates from the gaussian masking strategy.

(b) The evaluated bias voltage region originates from the fixed voltage masking strategy.

Figure 28: The bias voltage selection strategies for the impedance recovery are shown for the first two photon steps.

Pos. and Neg. Voltages	Gaussian Masking Limits		Defined Masking Limits	
	Y_{emb} [℧]	I_{LO} [µA]	Y_{emb} [℧]	I_{LO} [µA]
Skalare	0.0702 + 0.0586j	153.9	0.0705 + 0.0586j	154.4
Cost Function	0.0702 + 0.0586j	153.9	0.0702 + 0.0586j	153.9
Eyeball	0.1744 + 0.0857j	-0.01	0.1736 + 0.0863j	0.003
Withington	0.0702 + 0.0586j		0.0702 + 0.0586j	
Positive Voltages	Gaussian Masking Limits		Defined Masking Limits	
	Y_{emb} [℧]	I_{LO} [µA]	Y_{emb} [℧]	I_{LO} [µA]
Skalare	0.0697 + 0.0583j	153.0	0.0698 + 0.0584j	153.3
Cost Function	0.0697 + 0.0583j	153.0	0.0698 + 0.0584j	153.3
Eyeball	0.0714 + 0.0579	154.3	0.0664 + 0.0587	150.3
Withington	0.0697 + 0.0583j		0.0698 + 0.0584j	

Table 3: The results for the embedding admittance by using data from the first and second photon step show good results, except for the Eyeball method applied on negative and positive bias voltages.

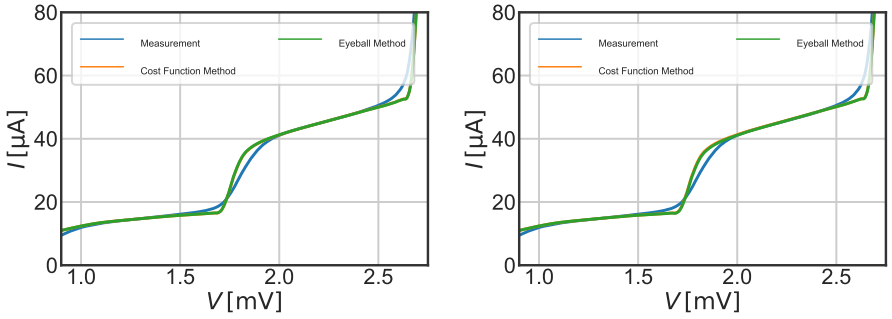

(a) The gaussian masking strategy on two photon steps.

(b) The fixed voltage range masking strategy on two photon steps.

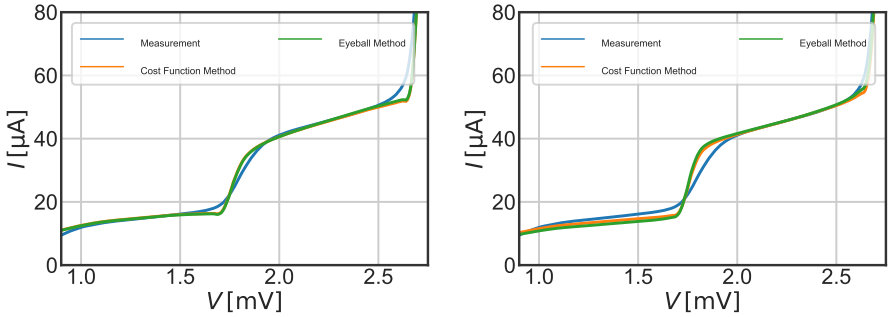

(c) This result is obtained from the extended voltage range of the fixed voltage range masking strategy, which includes the bias voltages between the first and second photon step.

(d) This result is obtained from the first photon step only and the fixed voltage masking strategy.

Figure 29: This figure compares the results obtained with different masking strategies applied on two photon steps (a-c) and one photon step (d). The results obtained in (a) and (b) are very similar, but both Eyeball evaluations fail as negative bias voltages are included in the evaluation.

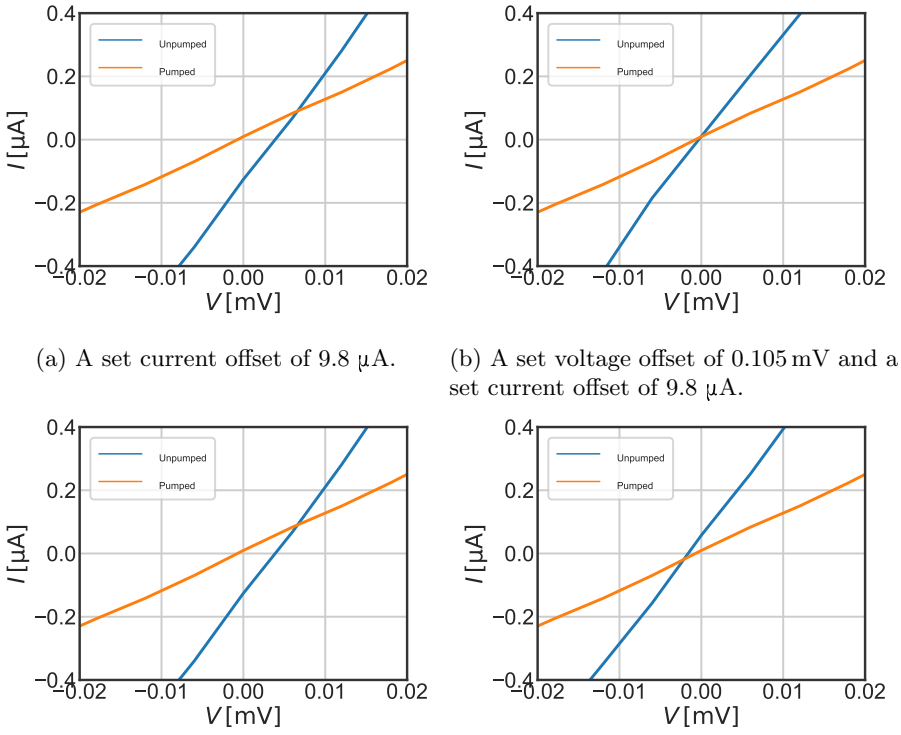

(a) A set current offset of 9.8 µA.

(b) A set voltage offset of 0.105 mV and a set current offset of 9.8 µA.

(c) A set current offset of 9.8 µA.

(d) The automatic offset correction by the `IV_Response` class.

Figure 30: This figure shows the offset of the unpumped and pumped IV curve close to the origin. The order corresponds with the order of table 4.

5 Discussion

In this final discussion section, the impact of the IV curve offset is discussed with respect to the discrepancy of our results to the QMix result. Figure 30 shows the origin of the measured IV curves with different offset settings and in figure 31, the corresponding recovered pumped IV curves are compared. The embedding admittances and impedances with respect to the photon step masking strategy and the used offset are listed in table 4. Note that the user define offset is applied on the unpumped IV curve only, and that the offset correction of the pumped IV curve is computed automatically in the `IV_Response` object following the description earlier. The voltage offset 0.101802 mV is determined by the `IV_Response` object on the unpumped IV curve. The offset has been partially chosen in a way to overlap the pumping level of the first photon step at negative and positive bias voltage regions as shown in figure 32.

The recovery of the pumped IV curve from the QMix embedding impedance

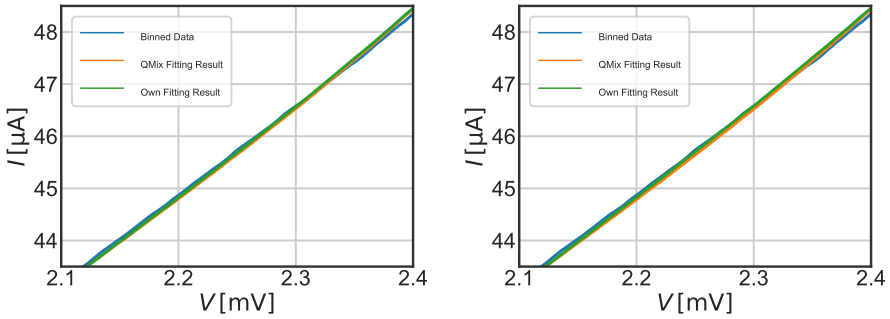

(a) A set current offset of 9.8 µA evaluated with the fixed masking strategy.

(b) A set voltage offset of 0.105 mV and current offset of 9.8 µA evaluated with the fixed masking strategy.

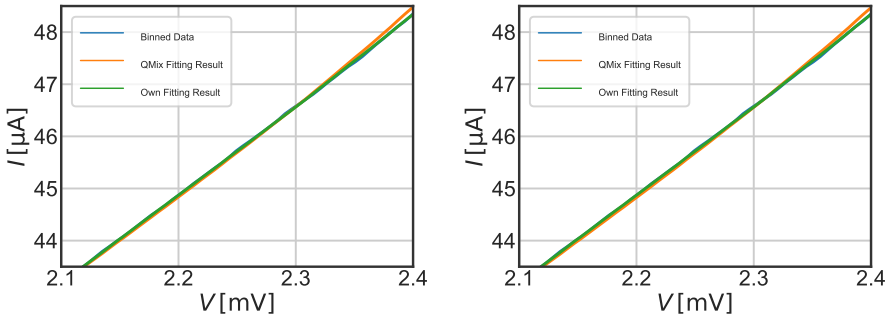

(c) A set current offset of 9.8 µA evaluated with the gaussian masking strategy.

(d) The automatic result with fixed masking strategy.

Figure 31: A comparison of the pumped IV curve recovered from the embedding admittance is shown for different IV curve offset settings at the first photon step. The QMix result varies, since during the recovery of the pumped IV curve the I_{LO} is computed from the masked pumping levels. A different masking strategy and a different voltage offset has impact on the I_{LO}. Note that the order corresponds with the order of table 4.

V_{offset}	I_{offset}	Masking Strategy	Y_{emb} [℧] Pos. & Neg. Bias	Y_{emb} [℧] Pos. Bias
0.101802	9.8	Fixed	0.1045+0.0705j	0.0955+0.0673j
0.105	9.8	Fixed	0.0949 + 0.0677j	0.0870 +0.0650j
0.101802	9.8	Gaus	0.0874 + 0.0631j	0.0797 + 0.0604
automatic	automatic	Fixed	0.1033 + 0.0703j	0.0950 + 0.0675j
V_{offset}	I_{offset}	Masking Strategy	Z_{emb} [Ω] Pos. & Neg. Bias	Z_{emb} [Ω] Pos. Bias
0.101802	9.8	Fixed	6.58-4.44j	6.99-4.93j
0.105	9.8	Fixed	6.98 - 4.98j	7.37 - 5.51j
0.101802	9.8	Gaus	7.52 - 5.43j	7.98 - 6.04j
automatic	automatic	Fixed	6.61 - 4.50j	6.99-4.97j

Table 4: The upper panel shows the embedding admittance results and the lower panel shows the embedding impedance results for different offset settings. The first entry in both panels has similar results as the QMix package and uses the same masking strategy as the QMix package. With respect to this, an additional voltage offset with the same masking strategy is evaluated, a result with gaussian masking strategy with the same offset as the first entry is evaluated, and finally an entry with the automatically calculated offset is given as comparison.

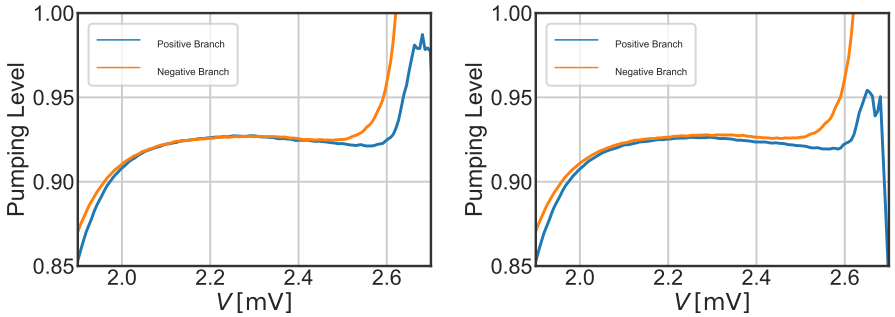

(a) A set current offset of 9.8 µA.

(b) A set voltage offset of 0.105 mV and a set current offset of 9.8 µA.

(c) A set current offset of 9.8 µA.

(d) The automatic offset correction by the `IV_Response` class.

Figure 32: The pumping level recovered from the unpumped and pumped IV curve are matched as a offset is introduced. Note that the order corresponds with the order of table 4.

result entails problems with the calculation of the I_{LO} following equation 11, since the equation contains the pumping level $V_{\mathrm{LO}}(V_0)$. The bias voltages used by the `Mixer` object at which the pumping level is determined must not be necessarily exactly the same as in the QMix package, even the fixed voltage masking strategy is used with the same limits as in the QMix package. A difference in the gap voltage give raise to an offset in the determined bias voltage range. For this reason, the recovered pumped IV curve from the QMix embedding impedance result vary with the offset on the IV curve data as well as with the used masking strategy for the photon step. This can be seen for instance in figure 31.

The four entries in figure 30, 31 and 32 and table 4 correspond in their order. The first entry is chosen to achieve a result for the embedding impedance close to the QMix result. As can be seen in figure 30, this result is not obtained at a perfect offset correction. The second entry introduced an additional voltage offset of about 0.003 mV to set the measured unpumped IV curve back to the origin. This, however, increases the result for the embedding impedance by $(0.40 - 0.44j)\,\Omega$. The third entry used the gaussian masking strategy on the offset settings of the first entry, and results in a larger magnitude for the embedding impedance. The last entry used the offset obtained from the `IV_Response` object of the unpumped IV curve. The difference in offset are additional 0.18 µA, which correspond with a difference of less than $(0.10 - 0.10j)\,\Omega$ in the embedding impedance results. In general, the result by evaluating only positive bias voltages results in larger embedding impedances.

The results of different masking strategies and evaluated voltages, applied on the first photon step in table 2, on two photon steps in table 3 and by introducing an offset in table 4, suggest that the impedance recovery can be seen as a rough guess value with a relative large error in the 10% regime. However, the recovered pumped IV curves show good agreement with the measured pumped IV curve in all cases. It is obvious that the IV curve offset has a strong impact on the pumping level and the following impedance recovery as shown in figure 32. In the same way, the impedance recovery result depends strongly on the bias voltage range in which the impedance recovery is performed. In general, the larger the bias voltage range, the smaller is the sensitivity of the recovery on noise. This noise can not only be introduced by the measurement, but also by physical backgrounds. An example is the Shapiro steps, which is negligible in the presented IV curves. Inclusion of data from the second photon step increases the bias voltage range used in the evaluation significantly. This, however, is not supported by literature and general practise. The inclusion of the photon steps at negative bias voltages is helpful in a way that the offset in the IV curve is accounted for. Nonetheless, this does not substitute the IV curve offset correction, since the pumping level recovery does not propagate the error linearly.

6 Conclusion

The presented software is able to determine the characteristic values of an IV response and the RF characteristics of a mixer. The used methods are described with references to the developed Python script. Testing and validation is obtained in conjunction with the QMix package. The results for the IV response agree with the exception of the subgap resistance, which can be ascribed to the different bias voltages evaluated. The obtained results for the embedding admittance agree with the measured data after recovering a pumped IV curve from the embedding admittance result in all cases. This leads to the conclusion that the recovered admittance is associated with large errors in the 10% regime. The strategies of selecting the bias voltage range on which the recovery is performed has certainly an impact on the result. In the same way, the result varies as photon steps only from positive bias voltages are considered or if also negative bias voltages are included in the computation. The inclusion of the second photon step leads to better agreement of the result with the measured pumped IV curve in the second photon step, while the result still agrees within the first photon step. Finally, the impact of the offset correction has been briefly discussed, which has an impact on the obtained result for the embedding admittance.

References

H. Rashid, V. Desmaris, A. Pavolotsky, and V. Belitsky. Harmonic and reactive behavior of the quasiparticle tunnel current in SIS junctions. *AIP Advances*, 2016. ISSN 21583226. doi: 10.1063/1.4947133.

A. Skalare. Determining embedding circuit parameters from DC measurements on quasiparticle mixers. *International Journal of Infrared and Millimeter Waves*, 1989. ISSN 01959271. doi: 10.1007/BF01010125.

J. R. Tucker and M. J. Feldman. Quantum detection at millimeter wavelengths. *Reviews of Modern Physics*, 1985. ISSN 00346861. doi: 10.1103/RevModPhys.57.1055.

S. Withington, K. G. Isaak, S. A. Kovtonyuk, R. A. Panhuyzen, and T. M. Klapwijk. Direct detection at submillimetre wavelengths using superconducting tunnel junctions. *Infrared Physics and Technology*, page 17, 1995. ISSN 13504495. doi: 10.1016/1350-4495(95)00058-5.